JACS
JOURNAL OF THE AMERICAN CHEMICAL SOCIETY

ARTICLE

pubs.acs.org/JACS

Nanostructures Boost the Thermoelectric Performance of PbS

Simon Johnsen,[†] Jiaqing He,[†,‡] John Androulakis,[†] Vinayak P. Dravid,[‡] Iliya Todorov,[§] Duck. Y. Chung,[§] and Mercouri G. Kanatzidis*[,†,§]

[†]Department of Chemistry, Northwestern University, Evanston, Illinois 60208, United States

[‡]Department of Materials Science and Engineering, Northwestern University, Evanston, Illinois 60208, United States

[§]Materials Science Division, Argonne National Laboratory, Argonne, Illinois 60439, United States

Supporting Information

ABSTRACT: In situ nanostructuring in bulk thermoelectric materials through thermodynamic phase segregation has established itself as an effective paradigm for optimizing the performance of thermoelectric materials. In bulk PbTe small compositional variations create coherent and semicoherent nanometer sized precipitates embedded in a PbTe matrix, where they can impede phonon propagation at little or no expense to the electronic properties. In this paper the nanostructuring paradigm is for the first time extended to a bulk PbS based system, which despite obvious advantages of price and abundancy, so far has been largely disregarded in thermoelectric research due to inferior room temperature thermoelectric properties relative to the pristine fellow chalcogenides, PbSe and PbTe. Herein we report on the synthesis, microstructural morphology and thermoelectric properties of two phase $(PbS)_{1-x}(PbTe)_x$ $x = 0-0.16$ samples. We have found that the addition of only a few percent PbTe to PbS results in a highly nanostructured material, where PbTe precipitates are coherently and semicoherently embedded in a PbS matrix. The present $(PbS)_{1-x}(PbTe)_x$ nanostructured samples show substantial decreases in lattice thermal conductivity relative to pristine PbS, while the electronic properties are left largely unaltered. This in turn leads to a marked increase in the thermoelectric figure of merit. This study underlines the efficiency of the nanostructuring approach and strongly supports its generality and applicability to other material systems. We demonstrate that these PbS-based materials, which are made primarily from abundant Pb and S, outperform optimally n-type doped pristine PbTe above 770 K.

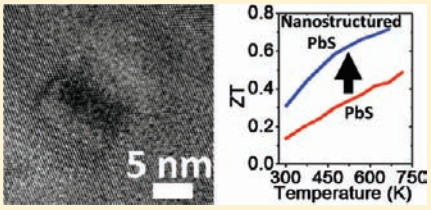

INTRODUCTION

The leading commercialized thermoelectric materials as well as those poised for commercialization in the near future are mainly telluride based[1−7] even though tellurium is extremely scarce in the Earth's crust.[8] Hence it would be desirable to develop alternative materials which minimize Te and involve cheaper and abundant elements. Currently bulk materials such as e.g. the filled skutterudites,[9−14] Zn_3Sb_4,[15−17] nanostructured Si and $Si_{1-x}Ge_x$,[18,19] half heuslers,[20−22] and $Mg_2Si_{1-x}Sn_x$[23,24] are being considered. Another possibility is PbS, also known as the mineral Galena, which is isostructural to PbTe adopting the rock salt structure with lattice parameters of 5.94 Å and 6.46 Å, respectively.[25] The electronic properties of the compounds are very similar. PbS has a reported room temperature band gap of 0.41 eV, whereas PbTe has a smaller gap of 0.32 eV.[26,27] Following the $10k_BT$ rule[28] this suggests PbS will show a maximum thermoelectric figure of merit (ZT) at higher temperatures than PbTe. Coupled with the significantly higher melting point of PbS (1391 K) in comparison with PbTe (1197 K) this implies that PbS-based thermoelectric materials have the potential to be used at higher temperatures. The room temperature effective mass of the conduction band is slightly higher in PbS than in PbTe.[26] Consequently, the reported electron mobilities are smaller in PbS, whereas the reported room temperature Seebeck coefficients for n-type PbS are higher at similar charge carrier concentration than in n-type PbTe.[26,29,30]

Despite the promising properties, surprisingly little research has been reported on the thermoelectric properties of bulk PbS compared to the isostructural PbTe. For the most part the literature is limited to studies at room temperature or below[31−33] although high-temperature Hall measurements and Seebeck coefficients have been reported.[29,34] The higher lattice thermal conductivity in this material in comparison to that of PbTe[26,35,36] impedes the attainment of a high ZT.

Nanostructuring has proven an efficient paradigm to lower lattice thermal conductivities and achieve higher ZT's in bulk thermoelectric materials.[37−40] Nanostructuring through nucleation and growth, spinodal decomposition, and matrix encapsulation is capable of not only lowering the lattice thermal conductivity significantly in PbTe[1,2] but also yielding improved power factors compared to those of the single-phase analogues.[4,5] Recently, the properties of several PbTe-rich compositions in the PbS−PbTe pseudobinary phase diagram were reported.[2] Due to an extensive immiscibility in this system, these samples are composite materials. The PbTe-rich part has shown nanometer-sized precipitates of PbS in a PbTe matrix, which gives a marked increase in the thermal resistivity of the composite at little cost to the electronic properties. Consequently a significant increase in ZT is observed at the optimized composition $PbTe_{0.92}S_{0.08}$.[2,41]

In this paper we report on the synthesis, microstructural morphology, and thermoelectric properties of the PbS-rich side of the pseudobinary PbS−PbTe phase diagram, which results in

Received: October 11, 2010
Published: February 18, 2011

dx.doi.org/10.1021/ja109138p | J. Am. Chem. Soc. 2011, 133, 3460–3470

materials with a PbS-rich major phase and a PbTe-rich minor phase. It is shown that the PbTe precipitates, formed even at very small concentrations of ~3 mol % and which range from several micrometers in size to a few nanometers, can significantly lower the lattice thermal conductivity in $PbS_{1-x}Te_x$ samples compared to that in pristine PbS at little cost to the electronic properties. As a result we demonstrate for the first time that the thermoelectric performance of n-type $(PbS)_{0.97}(PbTe)_{0.03}$ can exceed the ZT of optimized pristine PbTe (and PbS) above 770 K.

EXPERIMENTAL SECTION

Synthesis. In order to map out the effect of x on the lattice thermal conductivity in $PbS_{1-x}Te_x$, a range of undoped samples with $x = 0$, 0.01, 0.02, 0.03, 0.08, and 0.16 were synthesized. Furthermore, for the compositions $x = 0$, 0.03, 0.08, and 0.16 samples with 0, 0.033, 0.067, and 0.1 mol % $PbCl_2$ doping were synthesized to compare transport properties for different x and the determine the optimal doping level.

The samples were synthesized using the PbS and PbTe binaries in stoichiometric ratios. PbS was synthesized using elemental Pb (99.99% American Elements) and elemental S (99.985% 5N+) which was slowly heated to 720 K in 12 h, then heated to 1420 K in 6 h, soaked at this temperature for 6 h and subsequently cooled to room temperature. PbTe was synthesized using elemental Pb (99.99% American Elements) and elemental Te (99.999% 5N+), which was heated in a rocking furnace to 1320 K in 11 h, soaked for 6 h, and cooled to room temperature in 6 h. For the $PbS_{1-x}Te_x$ samples stoichiometric amounts of PbS and PbTe were mixed with 0.033−0.1 mol % of $PbCl_2$ (99.999% Aldrich) that was added as dopant. PbI_2 was initially chosen as a dopant but was not as effective as $PbCl_2$, possibly due to size mismatch of sulfur and iodine, which results in a lower solubility of PbI_2 in the lattice of PbS. The total sample mass was roughly 10 g; e.g. for the $x = 0.03$ sample with 0.1 mol % $PbCl_2$, 10.1192 g of PbS, 0.4379 g of PbTe, and 0.0121 g of $PbCl_2$ were used. The starting materials were loaded in a quartz ampule that subsequently was sealed under vacuum and reacted at 1423 K. From this temperature it was air quenched to room temperature followed by annealing for 3 days at 723 K. Carbon coating of the quartz ampule prevented side reactions with the quartz tube and was found to improve the mechanical strength of the samples. The ingots obtained were cut into coins of $\Phi \approx 8$ mm and 1−2 mm thickness for thermal diffusivity measurements and ~10 mm × 3 mm × 2 mm parallelepipeds that were used for simultaneous measurements of the Seebeck coefficient and the electrical conductivity. Examples of the obtained ingots and samples cut from them are shown in the Supporting Information.

Pristine PbS samples were synthesized in order to compare the properties with those of the $PbS_{1-x}Te_x$ samples. Attempts to make the sample in a similar way to the $PbS_{1-x}Te_x$ samples resulted in brittle samples with cracks and voids from which we were unable to obtain the dense specimens needed for transport properties measurement. Consequently, the pristine PbS samples were synthesized using vapor transport and Bridgman growth. For the former, PbS was sealed in evacuated silica tubes and kept for a week in a gradient of 1273 to 1323 K. The resulting transported material agglomerated in the cold end of the tube as an ingot with visible single-crystalline domains. From such domains sample coins could be cut for thermal diffusivity measurements and parallelepiped blocks of typical dimensions 10 mm × 3 mm × 2 mm for electronic properties measurements. Laue back reflection confirmed their single-crystalline nature (see Supporting Information for an example). Since samples had to be cut from a single-crystalline grain, for the vapor-transported samples it was not possible to measure thermal diffusivity and electronic properties along the same direction. Photographs of a representative sample are shown in the Supporting Information. The Bridgman grown samples were prepared using a single-zone furnace kept at 1423 K. PbS and $PbCl_2$ dopant was sealed in an evacuated quartz tube with a tapered end and lowered through the furnace at a rate of 2 mmh^{-1}. Coins for thermal diffusivity and parallelepipeds for electronic properties were cut in close proximity to minimize errors due to possible gradients in the dopant concentration, which can occur in Bridgman grown samples.[42] Transport properties were measured along the same direction for the Bridgman grown samples. Photographs of a representative sample are shown in the Supporting Information.

Physical Characterization. Thermal diffusivity was measured using a Netzsch LFA457 on the aforementioned coins cut from the sample. The samples were coated with a thin layer of graphite to minimize errors on the emissivity of the material. The data were analyzed using a Cowan model with pulse correction. Weighted combinations of literature values by Blachnik et al.[43] were used for the heat capacity. Using a Pyroceram 9606 standard this can also be determined from the thermal diffusivity data, and data were compared for consistency (shown in the Supporting Information). One sample was measured up to 920 K and a thin boron nitride coating was applied to eliminate thermal degradation of the sample. Seebeck coefficient and electrical conductivity were measured from room temperature to 720 K on ~10 mm × 3 mm × 2 mm parallelepipeds using an Ulvac Riko ZEM-3. One sample, which was measured to 920 K, was coated with a thin BN layer to avoid thermal degradation (see Supporting Information for photographs). Hall coefficients were measured on a home-built system in fields ranging from 0 to 1.25 T, utilizing a simple four-contact Hall-bar geometry, in both negative and positive polarity to eliminate Joule resistive errors. Diffuse reflectance measurements were conducted on a Thermo Nicolet 6700 FT-IR. Using the Kubelka−Munk function $(1 - R)^2/2R$, where R is the reflectance, the band gaps can be found by extending a fit to the linear region to the intersection with the x-axis.[44] Data were recorded on samples without added $PbCl_2$ dopant to minimize free carrier absorption. Scanning electron microscopy (SEM) was performed using a Hitachi S-3400N VP-SEM equipped with an Oxford detector for energy dispersive X-ray spectroscopy (EDS). The samples used for SEM and EDS were the coins used for thermal diffusivity, and they were polished using a suspension of 50 nm Al_2O_3 particles. Samples powdered in a agate mortar were used for powder X-ray diffraction on a CPS 120 Inel equipped with Cu Kα radiation. Scanning/transmission electron microscopy (S/TEM) investigations were carried out in a JEOL 2100F microscope operated at 200 kV. The thin TEM specimens were prepared by conventional standard methods, i.e., ground, dimpled, polished, and ion milled with liquid nitrogen.

RESULTS AND DISCUSSION

Compositional Characterization of the PbS-PbTe System. Lead sulfide and lead telluride form a continuous solid solution at temperatures above ~1100 K. Below this temperature an immiscibility dome forms that ranges from $x \approx 0.01$ to 0.96 at 673 K.[45,46] Within the immiscibility dome is a spinodal decomposition region, with no energy barrier to phase separation, and a nucleation and growth region where precipitation is energy activated. The exact borders of these regions are difficult to assign, but calculations show the spinodal region extends from $\sim 0.1 \leq x \leq \sim 0.82$ at 700 K.[46] The $PbS_{1-x}Te_x$ samples (where $x = 0-0.16$) presented in this study are therefore (for $x \geq 0.01$) expected to be composite materials with a continuous PbS-rich matrix containing PbTe-rich precipitates. This is confirmed by the powder X-ray diffraction patterns seen in Figure 1, where peaks from the PbS matrix and the PbTe precipitates are visible for $x > 0$. The composite nature of the material is also seen in the diffuse reflectance measurements. In Figure 1B the electronic absorption spectra are shown as a function of photon energy for the $x = 0$, 0.03, 0.08, and 0.16 samples. Here a band gap of 0.37 eV is observed for pure PbS, but with the addition of PbTe another gap appears at ~0.3 eV, consistent with the presence of PbTe as a

second phase. This is in agreement with the values of the optical band gap from spectroscopic absorption measurements of 0.32 eV for pure lead telluride and 0.41 eV for lead sulfide.[26] Similarly, SEM and EDS show a composite material with a PbS-rich major phase and PbTe-rich minor phase. This is evident in Figure 2, where precipitates are seen in the SEM images recorded using a secondary electron detector. EDS confirms that the major phase is PbS-rich with PbTe-rich precipitates. It is apparent from the SEM images that for x = 0.03 PbTe forms almost spherical isolated precipitates. For the x = 0.08 and 0.16 samples larger lamellar-shaped structures are formed. This is consistent with the expectation from the pseudobinary phase diagram:[45,46] the x = 0.03 sample at 773 K (temperature of the sample annealing) falls within the nucleation and growth region of the immiscibility dome, whereas the x = 0.16 composition lies within the spinodal decomposition region. The precipitate morphologies follow the expected trend.[2,41,47]

S/TEM studies on an undoped x = 0.03 sample show that in addition to the micrometer-sized precipitates observed in the SEM and EDS images there is a high density of nanosized precipitates ranging down to ~5 nm as shown in Figure 3. Since the PbTe precipitates are evenly dispersed throughout the PbS matrix and only present in a low concentration, spots due to the PbTe phase cannot be resolved in the electron diffraction pattern in Figure 3B. The precipitate shapes are very similar to the PbTe nanoprecipitates within larger PbS precipitates in $PbTe_{0.92}S_{0.08}$ and $PbTe_{0.7}S_{0.3}$.[41,47]

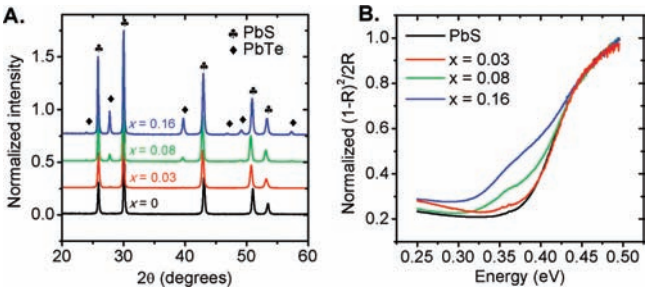

Figure 1. (A) Powder X-ray diffraction patterns of selected samples. Bragg peaks from PbS and PbTe are marked. (B) Electronic absorption spectra obtained from diffuse reflectance measurements on powdered $PbS_{1-x}Te_x$ samples.

Similarly for TEM studies on the undoped x = 0.16 sample there is a high density of nanosized precipitates ranging down to ~5 nm as shown in Figure 4. The precipitates are of two different kinds: one is lamellar shaped with large aspect ratios (Figure 4E and G), and the other is small and spherical-like (Figure 4 C, D, and F). These morphologies appear similar to the ones observed

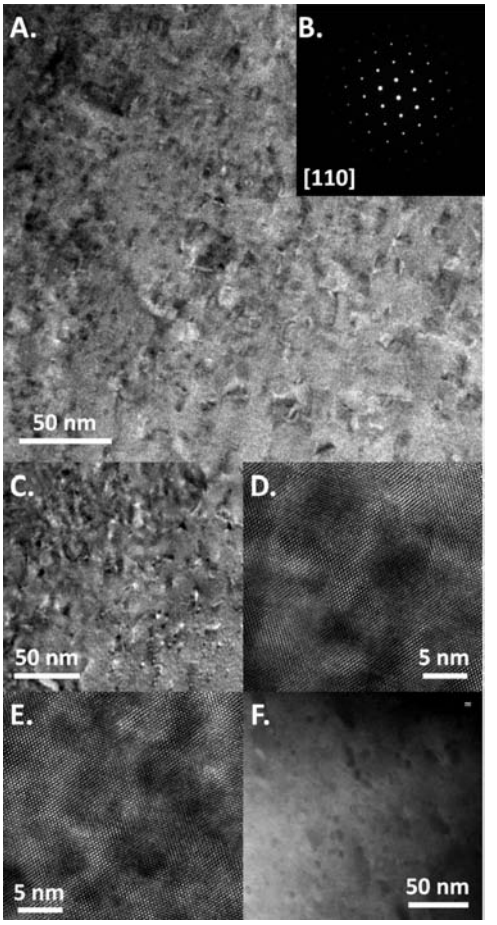

Figure 3. TEM images recorded on the undoped 3% sample. (A,C) Spherical-like nanocrystals dispersed evenly thoughout the PbS matrix. (B) Electron diffraction pattern recorded with an aperture which included the PbS matrix and the precipitates. (D,E) Precipitates at high magnification. (F) STEM image of same sample.

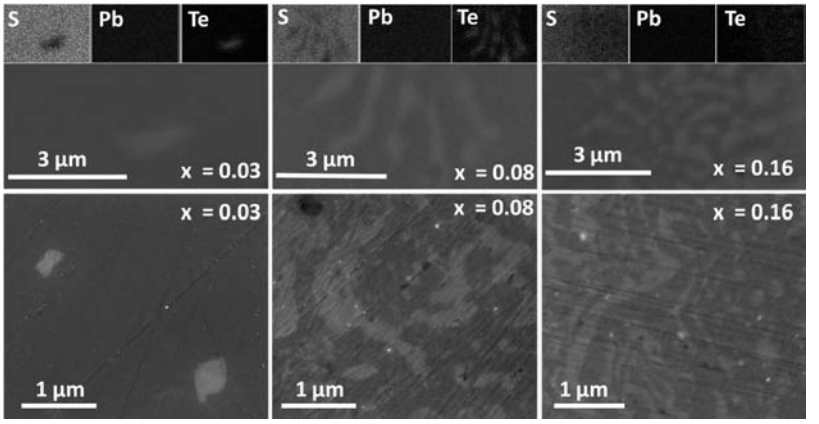

Figure 2. Scanning electron microscopy image of $PbS_{1-x}Te_x$ samples for x = 0.03, 0.08, and 0.16. Insets show element distribution determined by energy dispersive X-ray spectroscopy in the upper images.

dx.doi.org/10.1021/ja109138p | J. Am. Chem. Soc. 2011, 133, 3460–3470

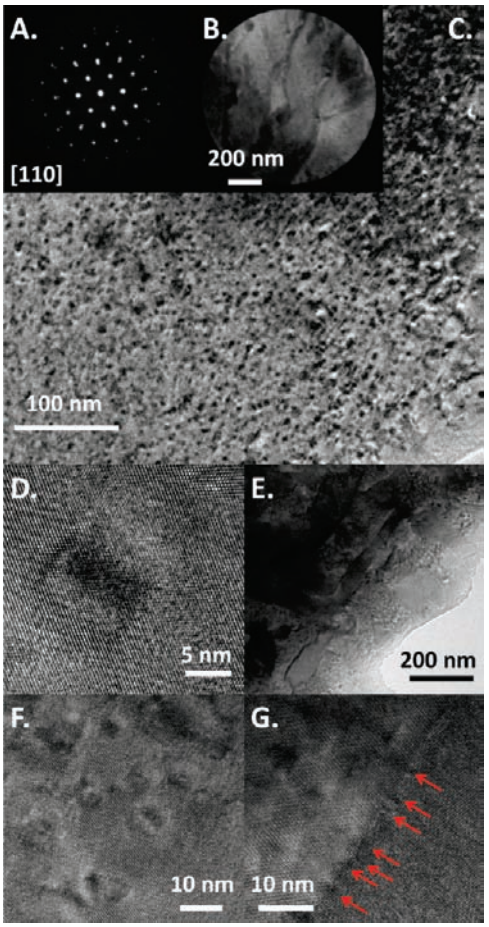

Figure 4. TEM studies of the undoped $x = 0.16$ sample. Two types of precipitates were detected: spherical-like precipitates (C, D, and E), and lamellar shaped precipitates (F and G). (A) Electron diffraction pattern using an aperture including the lamellar structures as shown in B.

in $PbS_{1-x}Te_x$ samples at the PbTe-rich side of the immiscibility dome, though on the PbTe-rich precipitates down to 2−3 nm precipitates are observed, whereas in the present PbS rich samples precipitates appear larger.[2,41,47] Figure 4A shows electron diffraction pattern of the PbS−PbTe interfaces using the selected area aperture seen in Figure 4B. The two separate phases can easily be identified by the split Bragg spots in the diffraction pattern due to the ∼8% difference in lattice parameters. Moreover the diffraction pattern reveals complete crystallographic alignment of the PbS and PbTe lattices. In order to release the strain from the mismatch in lattice parameter between PbS and PbTe, misfit dislocations are formed. This is evident in Figure 4G where dislocation cores along a PbS−PbTe boundary are marked by the red arrowheads.

Electronic Transport Properties. In the following, the transport properties of the $PbS_{1-x}Te_x$ samples will be analyzed with solutions to the Boltzmann transport equations within the relaxation time approximation. It is assumed the relaxation time, τ, has a simple power law dependence on the charge carrier energy, ε, so $\tau(T,\varepsilon) = \tau_0(T)\varepsilon^{\lambda-1/2}$, here τ_0 is the energy-independent term of the relaxation time, and λ is the scattering parameter. For acoustic phonon scattering $\lambda = 0$, and it will be assumed that this is the dominant scattering mechanism. Furthermore, electronic transport is assumed to be confined to a single parabolic band. The approach is described in detail by

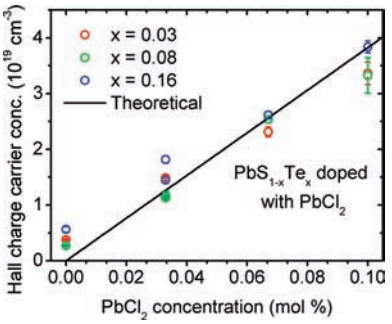

Figure 5. Hall charge carrier concentration in $PbS_{1-x}Te_x$ $x = 0.03$, 0.08, and 0.16 shown as a function of the added amount of $PbCl_2$. Solid line is the predicted carrier concentraion explained in the main text.

Fitsul'[48] and more recently for clathrate thermoelectric materials by May et al.[49] While the approximations we are making are valid for a single-phase homogeneous material, it will be shown that transport data for the present materials are described rather well.

The compositions $x = 0.03$, 0.08, and 0.16 were chosen for optimization of the carrier concentrations for reasons that will become clear in the discussion of the lattice thermal conductivity below.

Charge Carrier Concentration and Electron Mobilities. In the present $PbS_{1-x}Te_x$ samples $PbCl_2$ was used as a dopant. From simple valence counting each chlorine atom is expected to add one extra n-type carrier. In Figure 5 the room temperature Hall carrier concentrations are plotted as a function of the added amount of dopant. Here, the solid line represents one electron per chlorine atom added. It is seen that the amount of dopant scales as expected with the Hall charge carrier concentration within the error of measurement. The Hall measurements suggest that the maximum solubility of Cl has not been reached, and previous studies also suggest much higher Cl solubilities.[29,50]

Within the approximations outlined above, the Hall mobility can be expressed as:[48]

$$\mu_H = \frac{\theta\tau_0}{2m^*}\frac{F_{-1/2}(\eta)}{F_0(\eta)} \quad (1)$$

Here m^* is the effective mass of charge carriers, $F_n(\eta)$ are the Fermi integrals defined by May et al.[49] and evaluated for a specific reduced chemical potential, η, and

$$\tau_0 = \frac{\pi\hbar^4 C_{11}}{\sqrt{2}E_{def}(m^*kT)^{3/2}} \quad (2)$$

Here C_{11} is the longitudinal elastic constant, and E_{def} is the deformation potential. For a specific η the Hall mobility as calculated by eq 1 can be related to the Hall charge carrier concentration through:

$$n_H = 4\pi\left(\frac{2m^*kT}{h^2}\right)^{3/2}\frac{F_{1/2}(\eta)}{r_H} \quad (3)$$

Here r_H is the Hall factor defined by May et al.[49]

In Figure 6 the room temperature electron mobilities are plotted as a function of Hall charge carrier concentration. The solid line is calculated from eq 1. Here $\lambda = 0$ and with m^*, E_{def}, and C_{11} kept at the same values as in the evaluation of the conductivity below. From eq 2 this yields $\tau_0 = 1.6 \times 10^{-13}$ s (see

dx.doi.org/10.1021/ja109138p | J. Am. Chem. Soc. 2011, 133, 3460–3470

Electrical Conductivity section below for input values). Most samples follow the behavior expressed by the simple model due to eq 1. However, some $PbS_{1-x}Te_x$ samples fall well below the values expected by the model. This is attributed to microscopic cracks, grain boundaries, and defects leading to a higher residual resistance and, consequently, a lower Hall mobility. The Seebeck coefficient, however, is insensitive to these sample imperfections, and it will be shown below that it is well described by the simple parabolic band model.

Despite the composite nature of the $PbS_{1-x}Te_x$ samples, they do not show a dramatic decrease in the electron mobility in comparison with pristine PbS at similar charge carrier concentration. This can be seen by comparing, e.g. the $PbS_{1-x}Te_x$ samples with 0.033% $PbCl_2$ in Table 1 to the D and E PbS samples, which all exhibit similar charge carrier concentrations. All samples show mobilities around ~500 $cm^2 V^{-1} s^{-1}$ at 300 K. This is remarkable considering the high degree of micro- and nanostructuring in these composite $PbS_{1-x}Te_x$ samples as observed by SEM and high resolution TEM (see images in Figure 3 and Figure 4), which might be expected to decrease not only the phonon mean free path but also the charge carrier mobility. Previously, in PbTe, coherent and semicoherent nanostructures have proved efficient phonon scatterers with little or no impact on the charge carrier mobility.[1−3,S1] Considering the qualitative similarity in the nanostructures of the present PbS based materials with these PbTe systems little effect on the carrier mobility is expected, and these data provide further evidence for the efficiency of the nanostructuring paradigm. Below it is shown how the lattice thermal conductivity is reduced by up to 30% relative to PbS itself at room temperature by adding small amounts of PbTe. This has significant implications since these data suggests that the lattice thermal conductivity and

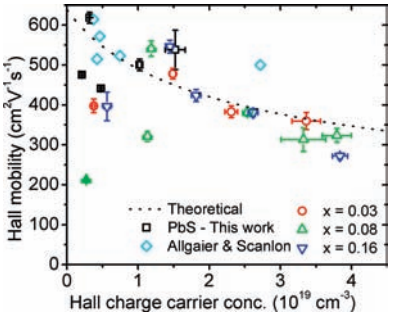

Figure 6. Room temperature Hall mobility for the $PbS_{1-x}Te_x$ as a function of the experimental Hall charge carrier concentration. Cyan diamonds are data by Allgaier and Scanlon.[59] Dotted line is due to the model described in the text.

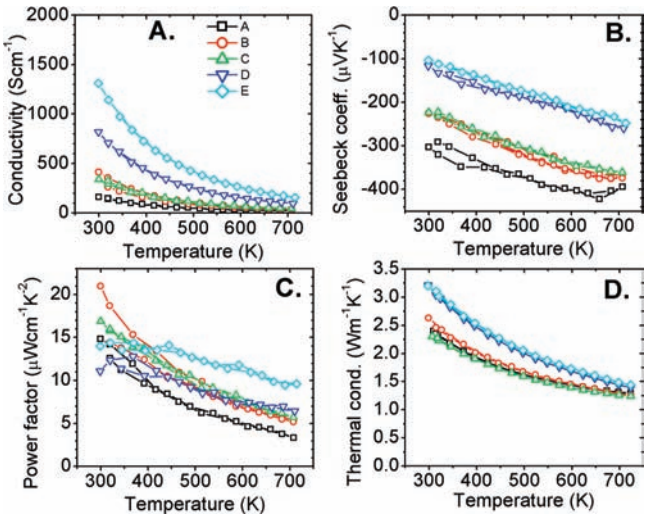

Figure 7. Thermoelectric properties of the pristine PbS samples. (A) Electrical conductivity as a function of sample temperature. (B) Seebeck coefficient as a function of sample temperature. (C) Thermoelectric powerfactor as a function of temperature. (D) Total thermal conductivity as function of temperature.

Table 1. Transport Properties of Selected $PbS_{1-x}Te_x$ Samples[a]

sample	n_H (10^{19} cm^{-3})	r_H	μ_H ($cm^2 V^{-1} s^{-1}$)	S ($\mu V K^{-1}$)	σ (S cm^{-1})	m^* (m_e)	κ_L(RT) (W $m^{-1} K^{-1}$)	κ_L(710 K) (W $m^{-1} K^{-1}$)
A[b]	0.21(2)	1.16	475	−303	161	0.57	2.38	1.28
B[b]	0.317(6)	1.14	618	−225	315	0.39	2.41	1.24
C[c]	0.480(6)	1.14	441	−223	339	0.51	2.19	1.20
D[c]	1.02(3)	1.08	500	−116	819	0.30	2.72	1.25
E[c]	1.52(14)	1.07	538	−103	1312	0.34	2.36	1.24
x = 0.03 undoped	0.37(2)	1.14	398	−223	240	0.43	1.94	1.09
x = 0.03 0.033% $PbCl_2$	1.48(4)	1.10	478	−137	1140	0.48	1.87	1.07
x = 0.03 0.067% $PbCl_2$	2.31(8)	1.06	383	−97	1417	0.41	1.98	1.10
x = 0.03 0.1% $PbCl_2$	3.4(2)	1.05	360	−76	1938	0.40	1.74	1.00
x = 0.08 undoped	0.271(4)	1.15	212	−254	92	0.45	1.85	1.08
x = 0.08 0.033% $PbCl_2$	1.18(4)	1.11	541	−134	1027	0.40	1.69	1.02
x = 0.08 0.067% $PbCl_2$	2.53(6)	1.06	381	−96	1549	0.44	1.74	1.06
x = 0.08 0.1% $PbCl_2$	3.3(3)	1.05	313	−78	1668	0.41	1.77	1.01
x = 0.16 undoped	0.56(5)	1.14	346	−227	357	0.39	1.66	1.04
x = 0.16 0.033% $PbCl_2$	1.44(4)	1.09	499	−133	1266	0.42	1.51	1.02
x = 0.16 0.067% $PbCl_2$	2.61(6)	1.06	289	−94	1594	0.43	1.65	1.00
x = 0.16 0.1% $PbCl_2$	3.83(11)	1.04	261	−72	1671	0.42	1.79	0.99

[a] Hall charge carrier concentration (n_H), Hall factor (r_H), Hall mobility (μ_H), Seebeck coefficient (S), electrical conductivity (σ) and effective mass (m^*) are shown at room temperature. Lattice thermal conductivity (κ_L) is shown at room temperature and 710 K. [b] The A and B were synthesized using vapor transport with no $PbCl_2$ added. [c] The C, D, and E samples were synthesized using the Bridgman method with 0.05, 0.1, and 0.2 mol % $PbCl_2$ added respectively.

dx.doi.org/10.1021/ja109138p | J. Am. Chem. Soc. 2011, 133, 3460–3470

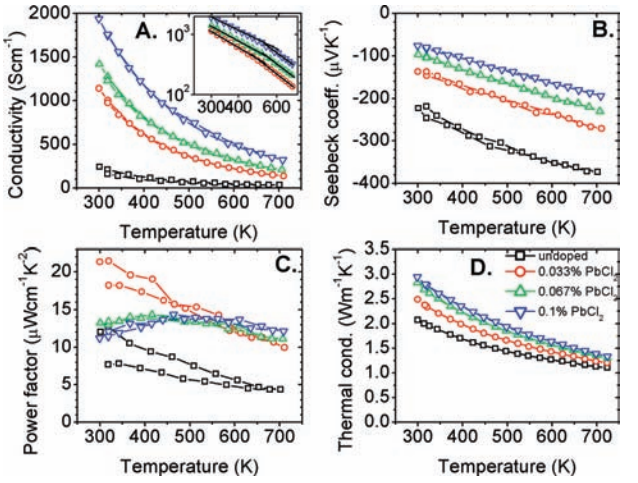

Figure 8. Thermoelectric properties of the x = 0.03 samples for different $PbCl_2$ doping. (A) Electrical conductivity as a function of sample temperature. Inset shows conductivity data for the doped samples on double logarithmic scales. (B) Seebeck coefficient as a function of sample temperature. (C) Thermoelectric powerfactor as a function of temperature. (D) Total thermal conductivity as function of temperature.

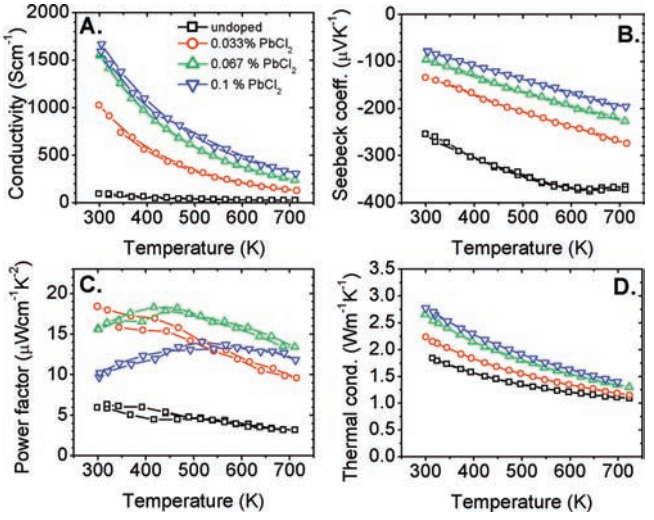

Figure 9. Thermoelectric properties of the x = 0.08 samples for different $PbCl_2$ doping. (A) Electrical conductivity as a function of sample temperature. (B) Seebeck coefficient as a function of sample temperature. (C) Thermoelectric powerfactor as a function of temperature. (D) Total thermal conductivity as function of temperature.

electronic properties can be varied independently in the $PbS_{1-x}Te_x$ materials.

Seebeck Coefficient. As expected the Seebeck coefficients (S) are negative and decreasing with the amount of added $PbCl_2$ (FigureS 7B−10B). The amount of dopant changes the temperature dependence from nondegenerate behavior in the samples with no added $PbCl_2$ (which from hereon will be referred to as undoped) to almost degenerate linear behavior of $S(T)$ in the case of the most heavily doped samples. For the x = 0.03 samples the undoped specimen has a room temperature Seebeck coefficient of $-223\ \mu V\ K^{-1}$ whereas the doped samples have $-137\ \mu V\ K^{-1}$, $-97\ \mu V\ K^{-1}$, and $-76\ \mu V\ K^{-1}$ as the $PbCl_2$ is increased from 0.033 mol % to 0.067 mol % and 0.1 mol % respectively.

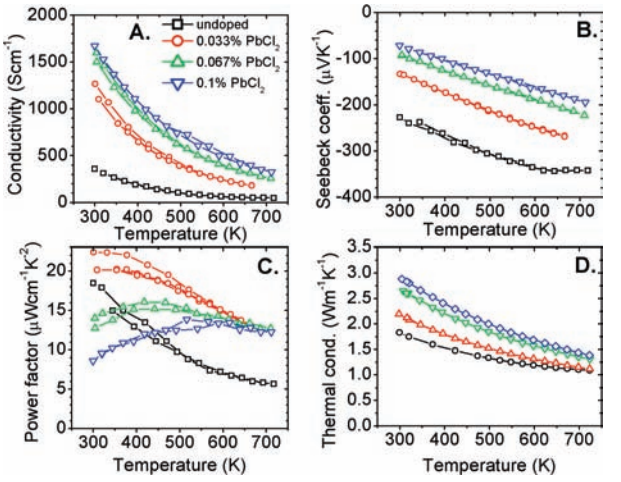

Figure 10. Thermoelectric properties of the x = 0.16 samples for different $PbCl_2$ doping. (A) Electrical conductivity as a function of sample temperature. (B) Seebeck coefficient as a function of sample temperature. (C) Thermoelectric powerfactor as a function of temperature. (D) Total thermal conductivity as function of temperature.

At 710 K the Seebeck coefficient ranges from $-373\ \mu V\ K^{-1}$ in the undoped sample showing signs of intrinsic conduction to $-194\ \mu V\ K^{-1}$ in 0.1 mol % $PbCl_2$ doped sample still dominated by extrinsic conduction. The same trend is seen in the x = 0.08 and 0.16 samples. The values for same dopant concentrations are identical within the error of measurement irrespective of x, which suggests the electronic transport is dominated by the PbS major phase. Table 1 shows a summary of the physical properties of selected samples and as expected increasing Hall charge carrier concentration leads to a lower absolute Seebeck coefficient.

Using the relation $E_g = 2eS_{max}T_{max}$,[52] where S_{max} is the maximum Seebeck coefficient and T_{max} is the corresponding temperature, the band gap can be determined for homogeneous semiconductors showing intrinsic conduction. This yields a band gap of ∼0.5 eV for pure PbS and ∼0.48 eV for the x = 0.08 samples, which again suggests the electronic properties are dominated by the PbS matrix, which has a larger band gap than PbTe. The x = 0.03 and 0.16 samples did not show clear minima in their Seebeck coefficient in the investigated temperature range of up to 710 K.

In the simple parabolic band model dominated by acoustic phonon scattering outlined above the Seebeck coefficient is given by:

$$S = \frac{k}{e}\left(\frac{2F_1(\eta)}{F_0(\eta)} - \eta\right) \qquad (4)$$

The Seebeck coefficient can for a specific η can be related to the Hall charge carrier concentration through eq 3 provided the effective mass, m^*, is known.

In Figure 11 the room temperature experimental Seebeck coefficients for all samples are plotted as a function of the Hall charge carrier concentration at room temperature. Data by Mal'tsev et al.[29] for pristine PbS doped with chlorine have been added for comparison. The solid lines are generated using eq 4 and related to n_H via eq 3 with effective masses of 0.3−0.5 m_e. Here m_e is the free electron mass. It is evident from Figure 11 that a parabolic band dominated by acoustic phonon scattering with an effective charge carrier mass of $m^* \approx 0.4\ m_e$ describes the

dx.doi.org/10.1021/ja109138p |J. Am. Chem. Soc. 2011, 133, 3460–3470

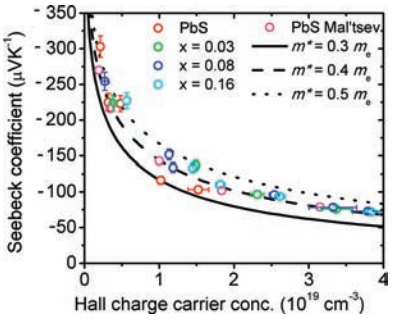

Figure 11. Room temperature Seebeck coefficients plotted as a function of Hall charge carrier concentration for the $PbS_{1-x}Te_x$ samples. Data for pristine PbS by Mal'tsev et al.[29] has been added for comparison. Lines are due to the model described in the main text.

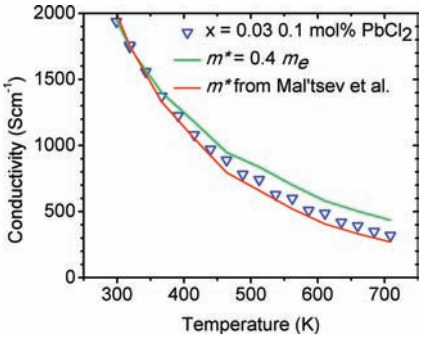

Figure 12. Conductivity of the $x = 0.03$ sample with 0.1% $PbCl_2$. Solid lines are due to the model described in the text. Green solid line is for m^* fixed at 0.4 m_e, while the solid red line takes into account the temperature dependence of m^* using data by Mal'tsev et al.[29].

experimental data rather well. Mal'tsev et al.[29] have previously reported the room temperature effective mass of pristine PbS (also obtained from Seebeck coeffients) to increase from 0.38 to 0.44 m_e as the charge carrier concentration increases from 4×10^{18} cm^{-3} to 7×10^{19} cm^{-3}. It is difficult to identify such a trend for the $PbS_{1-x}Te_x$ materials based on the current data.

Electrical Conductivity. In Figures 7A−10A the electrical conductivity (σ) data for the $x = 0$, 0.03, 0.08, and 0.16 samples are seen. As expected, there is an increase in $\sigma(T)$ within the amount of added dopant $PbCl_2$; e.g. for the $x = 0.03$ samples the conductivity at room temperature increases from 240 S cm^{-1} in the undoped sample to 1938 S cm^{-1} in the sample doped with 0.1 mol % $PbCl_2$. At 710 K the values are 31 S cm^{-1} and 320 S cm^{-1}, respectively. Since the conductivity scales with the amount of added dopant, this is an indication that the solubility limit of Cl has not been reached at 0.1 mol % as also observed in the determination of the Hall charge carrier concentration. There is good agreement between the measured Hall charge carrier concentrations listed in Table 1 and the room temperature σ, with higher carrier concentration resulting in higher electrical conductivity.

Whereas the electrical conductivity in n-type PbTe is effectively described by a power law of $\sigma \approx T^{-\delta}$ with $\delta = 2-2.5$ for doped specimens,[4,53] this is not the case for these doped composite PbS samples. This is evident from the inset in Figure 8 were the electrical conductivities of the doped $x = 0.03$ samples are plotted as a function of temperature on logarithmic scales. Here power law dependences show up as linear regions. No single power law can describe the data in the entire temperature range, but δ ranges from 1.8 at low temperature for samples with high dopant concentration to 2.8 at high temperature in samples with smaller dopant concentration. This is in part due to nondegenerate behavior and in part due to the strong temperature dependence of m^* above ∼400 K observed by Mal'tsev et al.[29]

Within the present single parabolic band approximation dominated by acoustic phonon scattering the electrical conductivity is given by:[48]

$$\sigma = \frac{8\pi e^2}{3m^* h^3}(2m^* kT)^{3/2}\tau_0 F_0(\eta) \qquad (5)$$

Here τ_0 is given by eq 2. Using the temperature-dependent ultrasonic studies by Chudinov,[54] $C_{11}(T)$ can be obtained from the sound velocity tensor. The measurements are limited to the temperature range 80−640 K, but extrapolation can be justified since the sound velocities vary linearly with temperature up to 640 K.[54] Ravich et al.[26] listed a room temperature deformation potential of ∼20 eV. Using the reduced chemical potentials obtained from the above fits to the Seebeck coefficient, an estimate of the temperature-dependent conductivity can be obtained from eq 5. In Figure 12 the experimental electrical conductivity of the $x = 0.03$ sample with 0.1% $PbCl_2$ is shown as a function of temperature along with the curve derived from eq 5. For the solid green line a temperature constant $E_{def} = 12.5$ eV was used, and m^* was fixed at 0.4 m_e. Although the model captures the general features of $\sigma(T)$, the experimental $\sigma(T)$ falls off more rapidly than that of the model. This could be due to the temperature dependences of E_{def} and m^*. Mal'tsev et al.[29] did find the conduction band effective mass to rise monotonically with temperature above 300 K, which could account for the divergence from the model since $\sigma \approx m^{*-1}$ from 5 and 6. Using the temperature dependence of the effective mass obtained by Mal'tsev et al.[29] a better agreement with data could be obtained (data for the sample 11 by Mal'tsev et al.[29] was used since it has a carrier density of 3.3×10^{19} cm^{-3} very similar to that of the present sample with a Hall charge carrier concentration of $3.4(2) \times 10^{19}$ cm^{-3}). This model, which takes the temperature dependence of the m^* into account, is shown by the red solid line in Figure 12. The data show that the evolution of the band structure with temperature in PbS has a significant impact on the charge transport properties and must be included in the modeling of transport data.

Power Factor and Thermal Stability. The high electrical conductivities and Seebeck coefficients combined give rise to high power factors of up to ∼22 μW cm^{-1} K^{-2} around room temperature and up to ∼13 μW cm^{-1} K^{-2} at 710 K (Figures 7C−10D). These power factor values are comparable to those obtained for PbTe-based materials at the same temperatures.[2] As expected, the maximum for the power factor is pushed to higher temperatures as the amount of dopant is increased. Whereas the $x = 0.03$, 0.08, and 0.16 samples doped with 0.033% $PbCl_2$ have their maxima near 300 K, the 0.067% $PbCl_2$ samples show a maxima at ∼450 K, and the 0.1% $PbCl_2$ samples show a maxima at ∼600 K. This implies that the temperature of optimum performance can conveniently be changed by varying the dopant concentration.

During the first run some irreversible behavior was seen in some of the samples and can probably be attributed to the loss of sulfur through evaporation from the surface layer. It has previously been reported that undoped high-resistance PbS crystals at temperatures higher than 700 K are subject to irreversible

changes in the resistivity and Hall coeffcient because of loss of sulfur through surface evaporation.[34] In our samples we observed that after continued thermal cycling the properties stabilize. Medium term thermal stability was tested for the $x = 0.03$ sample with 0.1 mol % $PbCl_2$. The sample was kept at 720 K for 4 h. No degradation of the sample was detectable within the error of the measurement. Data are shown in the Supporting Information. While this does not appear to be a problem for these n-type samples, it might be detrimental to the thermal stability of *p*-type samples, which could be driven n-type by the loss of sulfur. Preliminary trials with a protecting boron nitride coating show good thermal stability. The $x = 0.03$ sample with 0.1 mol % $PbCl_2$ was taken to 920 K. No discoloring of the BN coating nor degradation of the electronic properties was observed.

Thermal Conductivity. The total thermal conductivity (κ_{tot}) can be written as a sum of the electronic (κ_e) and lattice thermal conductivity (κ_L). The former is directly proportional to the electrical conductivity through the Wiedemann−Franz relation, $\kappa_e = L\sigma T$, where L is the Lorenz number.[48] On the other hand, κ_L is to a first approximation independent of the charge carrier concentration, though at high dopant concentration point defects due to dopant atoms is expected to lower κ_L. In a single band model when only one type of carriers are present L is easily calculated, and we will return to this below in the calculation of κ_L. At high temperature, when both holes and electrons are present, this relation breaks down since bipolar diffusion takes place, and an extra term then needs to be added to the total thermal conductivity.[55] It will be shown below that bipolar diffusion has little effect on the transport properties at these temperatures and doping levels. The proportionality of κ_e with σ is evident from the total thermal conductivities of the doped samples. As the amount of $PbCl_2$ is increased, κ_e increases along with σ; e.g. for the $x = 0.03$ samples (Figure 8D) κ increases from 2.07 W m^{-1} K^{-1} at room temperature (1.10 W m^{-1} K^{-1} at 723 K) in the undoped sample to 2.94 W m^{-1} K^{-1} at room temperature (1.34 W m^{-1} K^{-1} at 723 K) in the sample doped with 0.1% $PbCl_2$.

In the above assumption of a homogeneous material with a parabolic band dominated by acoustic phonon scattering the Lorenz number is given as:

$$L = \left(\frac{k}{e}\right)^2 \frac{3F_0(\eta)F_2(\eta) - 4F_1(\eta)^2}{F_0(\eta)^2} \qquad (6)$$

The reduced chemical potential η was obtained from fits to the experimental Seebeck coefficients using iterative fitting with eq 4. Using these η values, L for each sample can now be calculated and are shown in Figure 13 for the $x = 0.03$ samples. In the entire temperature range the Lorenz numbers are well below 2.45 × 10^{-8} W Ω K^{-2} for elastically scattered degenerate charge carriers. In estimations of the lattice thermal conductivities in thermoelectric systems the metallic limit of L is often used (i.e., 2.45 × 10^{-8} W Ω K^{-2}). In the present system this would grossly overestimate the electronic contribution to the thermal conductivity and hence underestimate the lattice contribution. It is evident from the listed κ_L's in Table 1 that the calculated L 's for the samples are close to the true Lorenz numbers since κ_L's for samples with different $PbCl_2$ doping and hence different κ_e's are in very good agreement. For wrong and too large Lorenz numbers, κ_e's would be overestimated, and there would be a systematic and substantial decrease in the calculated κ_L's with increasing $PbCl_2$ dopant. The trend in the calculated Lorenz

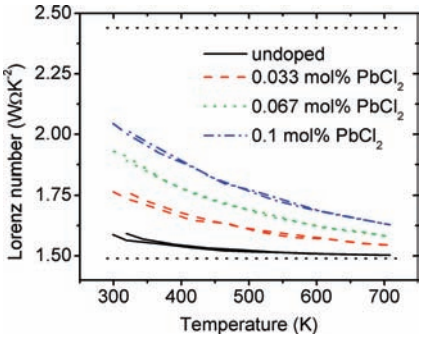

Figure 13. Calculated Lorenz numbers for the $x = 0.03$ samples with different carrier concentrations. Dotted horizontal lines correspond to degenerate (upper) and nondegenerate (lower) limits.

number in Figure 13 is consistent: The undoped sample is close to the nondegenerate limit, and with increasing amount of dopant the Lorenz number increases toward the degenerate limit.[48] For increasing temperature the Lorenz number decreases as η is decreasing.[48] At high temperature the single-band approximation can break down if the band gap is small enough to allow both holes and electrons to be present and bipolar diffusion to take place. False upturns in L at high temperature can then occur due to the failure of the single-band model.[49] No such upturn in L is observed for the $PbS_{1-x}Te_x$ samples, which shows that bipolar diffusion only has a minor effect on the transport properties for these doping levels and temperatures.

Nanostructured PbTe shows lattice thermal conductivities down to 0.4−0.5 W m^{-1} K^{-1} at 720 K, well below the values expected from the law of mixtures.[2,38,56] The nanostructures seen in the present PbS-rich samples are similar to the precipitate morphology in the PbTe-rich $PbS_{1-x}Te_x$ samples, where the semi-coherently or coherently embedded nanoprecipitates are efficient phonon scatterers.[2,41,47] Namely, there is a dramatic decrease in κ_L in going from a solid solution of $PbTe_{0.92}S_{0.08}$ to a two-phase nanostructured $(PbTe)_{0.92}(PbS)_{0.08}$.[41] Although the present $PbS_{1-x}Te_x$ materials show a high degree of nanostructuring, the reduction is not as dramatic as in PbTe, and at 710 K the minimum lattice thermal conductivity observed is 1.04 W m^{-1} K^{-1} in the $x = 0.16$ sample. This results in a 12%, 13%, and 16% decrease relative to the pristine PbS at 710 K. In $PbTe_{0.92}S_{0.08}$ where lattice thermal conductivities were dramatically reduced down to ∼0.4 W m^{-1} K^{-1} at 670 K[2] (this was calculated for $L = 2.45$ W Ω K^{-2}; however, with L calculated using η from the reported Seebeck coefficients $\kappa_L \approx 0.67$ W m^{-1} K^{-1}) the reduction at 670 K is 62% or 36% relative to pristine PbTe,[38] depending on whether 0.4 W m^{-1} K^{-1} or 0.67 W m^{-1} K^{-1} is used. Thus, it appears that nanosized precipitates of PbTe in PbS are not as effective phonon scatterers as PbS nanoprecipitates in PbTe. At present, the nature of this difference remains unclear, and detailed analysis of particle density and size distribution is required before a direct comparison can be made. Nevertheless, it appears that the nanoprecipitate size is slightly larger in the present PbS-rich samples in comparison to that in the PbTe-rich samples. For example, in the $x = 0.03$ sample the typical nanocrystal dimensions are ∼5−10 nm, whereas in $(PbTe)_{0.92}(PbS)_{0.08}$ they are 2−10 nm.[2,41] It can also be speculated whether the softer PbTe (Debye temperature θ_D = 130 K[26]) modes are more strongly scattered at the strained interfaces with energies more commensurate with the harder PbS modes ($\theta_D = 227$ K[26]). In Figure 14 κ_L's of the undoped $x = 0.03$,

dx.doi.org/10.1021/ja109138p |*J. Am. Chem. Soc.* 2011, 133, 3460–3470

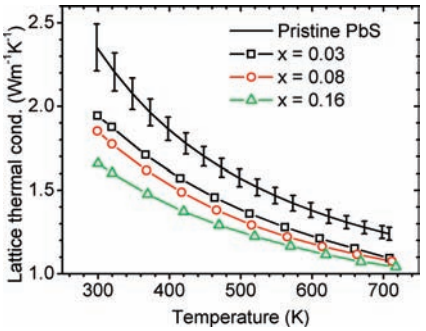

Figure 14. Temperature dependence of the lattice thermal conductivity of the $x = 0.03$, 0.08, and 0.16 samples. The mean of three different PbS samples is shown as the solid line. Error bars indicate the standard deviation for these samples.

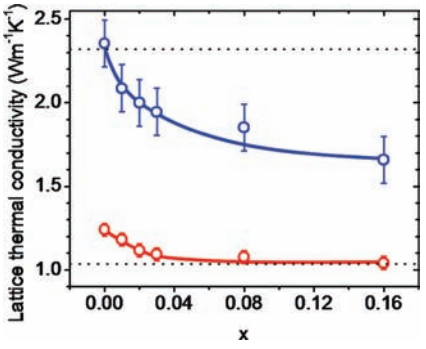

Figure 15. Lattice thermal conductivity of the undoped $PbS_{1-x}Te_x$ samples shown as a function of x at 300 K (blue) and 710 K (red). Solid lines are guide to the eye. The dotted horizontal lines are the lattice thermal conductivities of pristine PbTe at 300 K (upper) and 700 K (lower).[38].

0.08, and 0.16 samples are shown as function of temperature. The κ_L of pristine PbS is added for comparison, which is the average value determined from three separate samples. Error bars indicate the standard deviation on data from these three samples. In the entire temperature range there is a substantial decrease in κ_L over that of PbS for all $PbS_{1-x}Te_x$ samples.

One of the primary goals of this investigation was to determine the evolution of κ_L with changing x in $PbS_{1-x}Te_x$. In Figure 15 the lattice thermal conductivity at 300 and 710 K is plotted as a function of x. The lattice thermal conductivity was determined from measurements on undoped samples to minimize errors from wrongful determination of the electronic part. The Wiedemann–Franz relation was employed to calculate κ_e using the experimentally determined σ with the Lorenz number calculated as outlined in detail above. κ_L was then estimated using the relation $\kappa = \kappa_L + \kappa_e$. The error bar in Figure 15 for the pristine PbS is ± 1 standard deviation on three different samples. The same error was applied to the remaining data points. In PbTe the addition of 2% Sb or 1% CdTe results in a dramatic reduction of the high temperature κ_L.[56,57] Similarly in the $PbS_{1-x}Te_x$ samples there is a marked decrease in κ_L with the addition of even a few percent of PbTe at both 300 and 710 K. Increased PbTe addition in PbS beyond a few percent has a smaller effect, and the decrease in κ_L from $x = 0.03$ to 0.16 is less dramatic. The value of κ_L at 300 K and 700 K for pristine PbTe[38] is shown for comparison as the dashed and dotted line (this was calculated for a Lorenz number

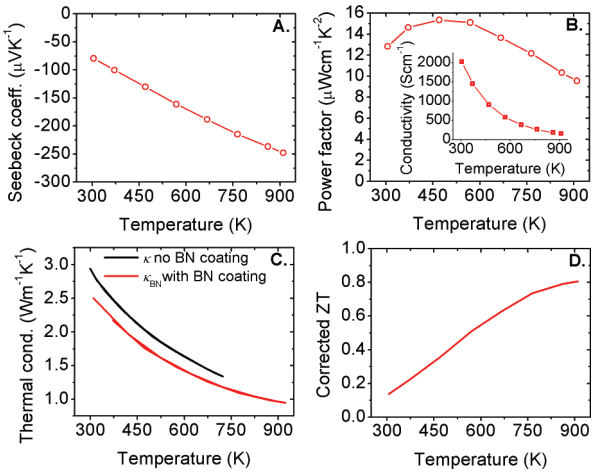

Figure 16. Transport properties of the BN-coated $x = 0.03$ sample with 0.1 mol % $PbCl_2$ measured to 920 K. (A). Seebeck coefficient as a function of temperature. (B) Power factor as a function of temperature; inset shows the electrical conductivity. (C) Total thermal conductivity of the sample with and without BN coating. (D) ZT of the sample after correction of the total thermal conductivity.

of 2.45×10^{-8} Ω W K^{-2} which leads to a slightly underestimated κ_L, see discussion above). At room temperature there is a 30% decrease of the lattice thermal conductivity in going from pristine PbS to the $x = 0.16$ sample (17% and 21% for the $x = 0.03$ and 0.08 sample, respectively). This is a considerable decrease, considering the electronic properties are largely left unaltered as shown above in the discussion of electron mobility, Seebeck coefficient, and electrical conductivity. Relative to pristine PbS there is a significant drop in κ_L at 710 K, which amounts to up to 16% for the $x = 0.16$ sample. The drop in κ_L upon addition of small PbTe amounts ($x \approx 0.16$) brings κ_L of PbS to the level of that of pristine PbTe.

Thermoelectric Figure of Merit. For the $x = 0.03$ samples the 0.1 mol % $PbCl_2$ doped exhibit the highest figure of merit at 710 K, yet the ZT has not reached its maximum at this temperature. Consequently, this sample was measured to 920 K. In order to avoid the thermal degradation observed by Scanlon[34] the sample was coated with a thin BN layer. These properties are shown in Figure 16. The total thermal conductivity measured with the BN coating (κ_{BN}) is underestimated compared to the previous measurement without BN coating (κ), probably due to increased thermal resistivity from the encapsulating BN layer. At 720 K the difference is $\kappa/\kappa_{BN} = 1.13$. This factor was used to correct the data up to 920 K. It is evident from the temperature dependence, where κ decreases more rapidly than κ_{BN}, that this ratio is probably smaller at 920 K, so the corrected value of κ_{BN} can be regarded as an upper limit. Using the corrected κ_{BN} value and the power factor in Figure 16 the remarkably high ZT = 0.81 at 910 K for a PbS-based material is obtained.

Figure 17 shows the $PbS_{1-x}Te_x$ samples with the highest ZT's. Data for optimally doped pristine PbTe is also shown for comparison.[58] The pristine PbS with the highest ZT reaches only 0.5 at 710 K. This sample has a charge carrier concentration similar to those of the $PbS_{1-x}Te_x$ samples doped with 0.033 mol % $PbCl_2$. It is seen that all the $PbS_{1-x}Te_x$ samples show ZT's which are markedly increased over that of the parent material PbS and approach the values for n-type pristine PbTe at 670 K,

dx.doi.org/10.1021/ja109138p | J. Am. Chem. Soc. 2011, 133, 3460–3470

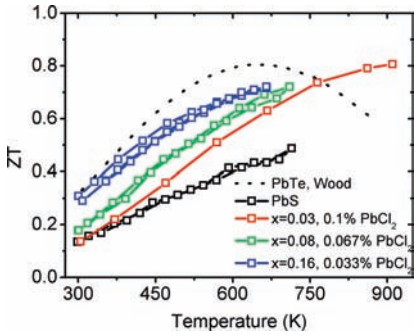

Figure 17. Dimensionless thermoelectric figure of merit for the best $PbS_{1-x}Te_x$ samples. Literature values for optimally doped pristine n-type PbTe are added for comparison.[58]

where PbTe shows its ZT maximum. The $x = 0.03$ sample with 0.1 mol % $PbCl_2$ outperforms PbTe above ~770 K and continues to increase until the last measured temperature 920 K, where it reaches 0.81. For the $x = 0.08$ sample with 0.067 mol % $PbCl_2$ the ZT increases from 0.18 at room temperature to 0.72 at 710 K. This corresponds to a 48% increase relative to the PbS sample at the same temperature. High room temperature power factors and the low lattice thermal conductivity give the $x = 0.16$ sample with 0.033 mol % $PbCl_2$ not only a high ZT of 0.72 at 665 K but also a room temperature ZT of 0.3, which matches that of the pristine PbTe. This is of importance in device applications where a high ZT is required over as broad a temperature range as possible. At 710 K the optimal doping level is between 0.033 and 0.067 mol % $PbCl_2$. Generally, in the former case (0.033 mol % $PbCl_2$) the power factors are smaller, but this is compensated by the smaller electronic thermal conductivity. In the latter case (0.067 mol % $PbCl_2$) the power factors are higher, but so is the electronic thermal conductivity. At 910 K the $x = 0.03$ sample with 0.1% $PbCl_2$ is close to optimally doped.

CONCLUSIONS

We have shown that composite sulfur-rich $PbS_{1-x}Te_x$ samples can be successfully synthesized and grown as high-quality crystalline ingots. The addition of only a few percent of PbTe into PbS generates nanostructring which produces a reduction of the lattice thermal conductivity compared to pristine PbS, but without significantly altered electronic properties. This leads to a marked increase in the ZT values compared to those of pristine PbS of ~50% at 710 K. Despite the composite nature of these $PbS_{1-x}Te_x$ materials their electronic properties are remarkably well described using the assumption of homogeneous material dominated by a single parabolic band under the influence of acoustic phonon scattering. Above ~770 K the composite samples outperform pristine PbTe and reach ZT ≈ 0.8 at 910 K. Since these materials are made primarily from abundant Pb and S, they provide a cheap alternative to PbTe, which albeit being a high performance thermoelectric material, may have difficulties finding widespread use due to the scarcity and price of Te.

Compared to the large reductions of 40% in κ_L observed in $(PbTe)_{0.92}(PbS)_{0.08}$ relative to those in PbTe at high temperature, the 16% decrease observed in the present samples relative to PbS suggests there is significant room for improvement. If the PbTe precipitate size can be controlled and decreased, a further reduction of the lattice thermal conductivity is feasible. Provided a 40% decrease can be achieved relative to PbS, ZT of 0.94 at 710 K (electronic data for the $x = 0.08$ with 0.067 mol % $PbCl_2$) is obtained. Traditional approaches such as increased thermal resistance through solid solution with, e.g., PbSe could be used in combination with the present nanostructuring to further boost the ZT. Another approach could be an increase in the power factor through the incorporation of elements forming resonance states such as Tl. Hence, there is room for further optimization, and it appears feasible to obtain PbS-based thermoelectric materials with ZT > 1 at 900 K.

ASSOCIATED CONTENT

Supporting Information. Photographs of the samples and different stages in the sample preparation (Figures S1 and S2); Laue photograph of a vapor grown PbS sample (Figure S3); Figure S4 shows the boron nitride coating of a sample for high-temperature measuremets; Figures S5−S8 show the thermal diffusivity of all samples, and Figures S10−S13, their measured heat capacity from the thermal diffusivity measurements using a pyroceram 9606 standard; Figure S9 shows the model heat capacity used for the different samples, and the supporting text describes how this was calculated for literature data; the model data are included in Figures S10−S13 for comparison; Figures S14 and S15 show the time evolution of the Seebeck coefficient and electrical conductivity for samples kept at 710 K for 4 h; Table S1 shows the measured density of all samples. This material is available free of charge via the Internet at http://pubs.acs.org.

AUTHOR INFORMATION

Corresponding Author
m-kanatzidis@northwestern.edu

ACKNOWLEDGMENT

S.J. acknowledges funding from the Danish Council for Independent Research, Natural Sciences. This material is based upon work supported as part of the Revolutionary Materials for Solid State Energy Conversion, an Energy Frontier Research Center funded by the U.S. Department of Energy, Office of Science, Office of Basic Energy Sciences under Award Number DE-SC0001054. This work was also supported by the U.S. Department of Energy, Office of Science under Contract No. DE-AC02-06CH11357.

REFERENCES

(1) Hsu, K. F.; Loo, S.; Guo, F.; Chen, W.; Dyck, J. S.; Uher, C.; Hogan, T.; Polychroniadis, E. K.; Kanatzidis, M. G. *Science* **2004**, *303*, 818.

(2) Androulakis, J.; Lin, C. H.; Kong, H. J.; Uher, C.; Wu, C. I.; Hogan, T.; Cook, B. A.; Caillat, T.; Paraskevopoulos, K. M.; Kanatzidis, M. G. *J. Am. Chem. Soc.* **2007**, *129*, 9780.

(3) Poudeu, P. F. R.; D'Angelo, J.; Downey, A. D.; Short, J. L.; Hogan, T. P.; Kanatzidis, M. G. *Angew. Chem., Int. Ed.* **2006**, *45*, 3835.

(4) Sootsman, J. R.; Kong, H.; Uher, C.; D'Angelo, J. J.; Wu, C. I.; Hogan, T. P.; Caillat, T.; Kanatzidis, M. G. *Angew. Chem., Int. Ed.* **2008**, *47*, 8618.

(5) Heremans, J. P.; Thrush, C. M.; Morelli, D. T. *Phys. Rev. B* **2004**, *70*, 115334.

(6) Heremans, J. P.; Jovovic, V.; Toberer, E. S.; Saramat, A.; Kurosaki, K.; Charoenphakdee, A.; Yamanaka, S.; Snyder, G. J. *Science* **2008**, *321*, 554.

(7) Gelbstein, Y.; Dado, B.; Ben-Yehuda, O.; Sadia, Y.; Dashevsky, Z.; Dariel, M. P. *J. Electron. Mater.* **2010**, *39*, 2049.
(8) Hu, Z. C.; Gao, S. *Chem. Geol.* **2008**, *253*, 205.
(9) Morelli, D. T.; Meisner, G. P. *J. Appl. Phys.* **1995**, *77*, 3777.
(10) Sales, B. C.; Mandrus, D.; Williams, R. K. *Science* **1996**, *272*, 1325.
(11) Shi, X.; Kong, H.; Li, C. P.; Uher, C.; Yang, J.; Salvador, J. R.; Wang, H.; Chen, L.; Zhang, W. *Appl. Phys. Lett.* **2008**, *92*, 182101.
(12) Nolas, G. S.; Kaeser, M.; Littleton, R. T.; Tritt, T. M. *Appl. Phys. Lett.* **2000**, *77*, 1855.
(13) Tang, X. F.; Li, H.; Zhang, Q. J.; Niino, M.; Goto, T. *J. Appl. Phys.* **2006**, *100*, 123702.
(14) Zhao, W. Y.; Wei, P.; Zhang, Q. J.; Dong, C. L.; Liu, L. S.; Tang, X. F. *J. Am. Chem. Soc.* **2009**, *131*, 3713.
(15) Snyder, G. J.; Christensen, M.; Nishibori, E.; Caillat, T.; Iversen, B. B. *Nat. Mater.* **2004**, *3*, 458.
(16) Caillat, T.; Fleurial, J. P.; Borshchevsky, A. *J. Phys. Chem. Solids* **1997**, *58*, 1119.
(17) Nylen, J.; Andersson, M.; Lidin, S.; Haussermann, U. *J. Am. Chem. Soc.* **2004**, *126*, 16306.
(18) Bux, S. K.; Blair, R. G.; Gogna, P. K.; Lee, H.; Chen, G.; Dresselhaus, M. S.; Kaner, R. B.; Fleurial, J. P. *Adv. Funct. Mater.* **2009**, *19*, 2445.
(19) Joshi, G.; Lee, H.; Lan, Y. C.; Wang, X. W.; Zhu, G. H.; Wang, D. Z.; Gould, R. W.; Cuff, D. C.; Tang, M. Y.; Dresselhaus, M. S.; Chen, G.; Ren, Z. F. *Nano Lett.* **2008**, *8*, 4670.
(20) Culp, S. R.; Poon, S. J.; Hickman, N.; Tritt, T. M.; Blumm, J. *Appl. Phys. Lett.* **2006**, *88*, 042106.
(21) Mastronardi, K.; Young, D.; Wang, C. C.; Khalifah, P.; Cava, R. J.; Ramirez, A. P. *Appl. Phys. Lett.* **1999**, *74*, 1415.
(22) Sakurada, S.; Shutoh, N. *Appl. Phys. Lett.* **2005**, *86*, 082105.
(23) Zaitsev, V. K.; Fedorov, M. I.; Gurieva, E. A.; Eremin, I. S.; Konstantinov, P. P.; Samunin, A. Y.; Vedernikov, M. V. *Phys. Rev. B* **2006**, *74*, 045207.
(24) Nikitin, E. N.; Bazanov, V. G.; Tarasov, V. I. *Soviet Phys. Solid State (Engl. Transl.)* **1962**, *3*, 2648.
(25) Madelung, O. *Semiconductors: Data Handbook*, 3rd ed.; Springer: Berlin, 2004.
(26) (a) Ravich, Y. I.; Efimova, B. A.; Smirnov, I. A. *Semiconducting Lead Chalcogenides*; Plenum Press: New York, London, 1970. (b) Han, M. K.; Hoang, K.; Kong, H. J.; Pcionek, R.; Uher, C.; Paraskevopoulos, K. M.; Mahanti, S. D.; Kanatzidis, M. G. *Chem. Mater.* **2008**, *20*, 3512. (c) Ahn, K.; Li, C. P.; Uher, C.; Kanatzidis, M. G. *Chem. Mater.* **2009**, *21*, 1361.
(27) Scanlon, W. W. *J. Phys. Chem. Solids* **1959**, *8*, 423.
(28) Mahan, G. D. *Solid State Phys.* **1998**, *51*, 81.
(29) Maltsev, Y. V.; Nensberg, E. D.; Petrov, A. V.; Semiletov, S. A.; Ukhanov, Y. I. *Sov. Phys. Solid State (Engl. Transl.)* **1967**, *8*, 1713.
(30) Wright, D. A. *Metall. Rev.* **1970**, *15*, 147.
(31) Finlayson, D. M.; Greig, D. *Proc. Phys. Soc. London* **1959**, *73*, 49.
(32) Greig, D. *Phys. Rev.* **1960**, *120*, 358.
(33) Harman, T. C.; Strauss, A. J. *J. Electron. Mater.* **1976**, *5*, 621.
(34) Scanlon, W. W. *Phys. Rev.* **1953**, *92*, 1573.
(35) El-Sharkawy, A. A.; Abou El-Azm, A. M.; Kenawy, M. I.; Hillal, A. S.; Abu-Basha, H. M. *Int. J. Thermophys.* **1983**, *4*, 261.
(36) Alekseeva, G. T.; Vinogradova, M. N.; Gartsman, K. G.; Zyuzin, A. Y.; Mailina, K. P.; Prokofeva, L. V.; Stilbans, L. S. *Fizika Tverdogo Tela* **1985**, *27*, 3242.
(37) Snyder, G. J.; Toberer, E. S. *Nat. Mater.* **2008**, *7*, 105.
(38) Sootsman, J. R.; Chung, D. Y.; Kanatzidis, M. G. *Angew. Chem., Int. Ed.* **2009**, *48*, 8616.
(39) (a) Kanatzidis, M. G. *Chem. Mater.* **2010**, *22*, 648. (b) Vineis, C. J.; Shakouri, A.; Majumdar, A.; Kanatzidis, M. G. *Adv. Mater.* **2010**, *22*, 3970.
(40) Dresselhaus, M. S.; Chen, G.; Tang, M. Y.; Yang, R. G.; Lee, H.; Wang, D. Z.; Ren, Z. F.; Fleurial, J. P.; Gogna, P. *Adv. Mater.* **2007**, *19*, 1043.
(41) Girard, S. N.; He, J.; Li, C.; Moses, S.; Wang, G.; Uher, C.; Dravid, V. P.; Kanatzidis, M. G. *Nano Lett.* **2010**, *10*, 2825.
(42) Pamplin, B. R. *Crystal Growth*; Pergamon Press: Oxford, 1975.
(43) Blachnik, R.; Igel, R. *Z. Naturforsch., B: Chem. Sci.* **1974**, *B 29*, 625.
(44) (a) Tandon, S. P.; Gupta, J. P. *Phys. Status Solidi* **1970**, *38*, 363. (b) Liao, J. H.; Kanatzidis, M. G. *J. Am. Chem. Soc.* **1990**, *112*, 7400. (c) McCarthy, T. J.; Kanatzidis, M. G. *Chem. Mater.* **1993**, *5*, 1061. (d) Chen, B. X.; Uher, C.; Iordanidis, L.; Kanatzidis, M. G. *Chem. Mater.* **1997**, *9*, 1655.
(45) Darrow, M. S.; White, W. B.; Roy, R. *Trans. Metall. Soc. AIME* **1966**, *236*, 654.
(46) Volykhov, A. A.; Yashina, L. V.; Shtanov, V. I. *Inorg. Mater.* **2006**, *42*, 596.
(47) He, J. Q.; Girard, S. N.; Kanatzidis, M. G.; Dravid, V. P. *Adv. Funct. Mater.* **2010**, *20*, 764.
(48) Fitsul', V. I. *Heavily Doped Semiconductors*; Plenum Press: New York, 1969.
(49) May, A. F.; Toberer, E. S.; Saramat, A.; Snyder, G. J. *Phys. Rev. B* **2009**, *80*, 125205.
(50) Alekseeva, G. T.; Veis, A. N.; Gurieva, E. A.; Zhukova, T. B.; Prokofeva, L. V. *Sov. Phys. Semicond.* **1990**, *24*, 1336.
(51) Poudeu, P. F. P.; D'Angelo, J.; Kong, H. J.; Downey, A.; Short, J. L.; Pcionek, R.; Hogan, T. P.; Uher, C.; Kanatzidis, M. G. *J. Am. Chem. Soc.* **2006**, *128*, 14347.
(52) Goldsmid, H. J.; Sharp, J. W. *J. Electron. Mater.* **1999**, *28*, 869.
(53) Ravich, Y. I.; Efimova, B. A.; Tamarche, V. I. *Phys. Status Solidi B* **1971**, *43*, 11.
(54) Chudinov, A. A. *Sov. Phys. Solid State (Engl. Transl.)* **1963**, *5*, 1061.
(55) Bhandari, C. M.; Rowe, D. M. *Thermal Conduction in Semiconductors*; Wiley: New Delhi, 1988.
(56) Sootsman, J. R.; Pcionek, R. J.; Kong, H. J.; Uher, C.; Kanatzidis, M. G. *Chem. Mater.* **2006**, *18*, 4993.
(57) Ahn, K.; Han, M. K.; He, J. Q.; Androulakis, J.; Ballikaya, S.; Uher, C.; Dravid, V. P.; Kanatzidis, M. G. *J. Am. Chem. Soc.* **2010**, *132*, 5227.
(58) Wood, C. *Rep. Prog. Phys.* **1988**, *51*, 459.
(59) Allgaier, R. S.; Scanlon, W. W. *Phys. Rev.* **1958**, *111*, 1029.